TÉCNICO LISBOA

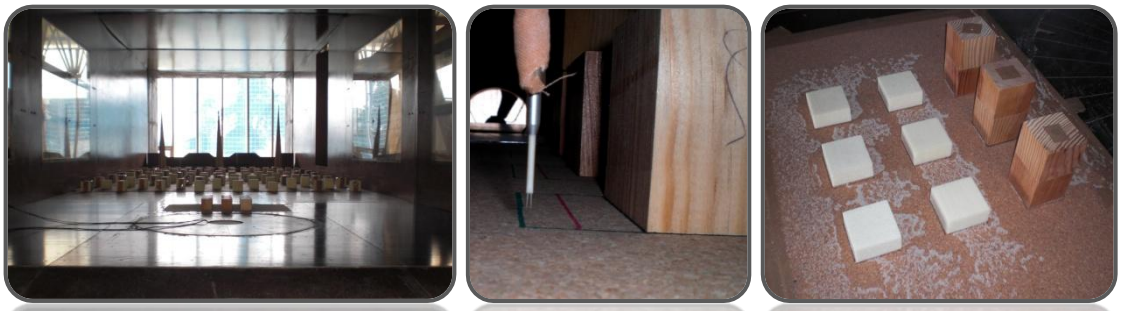

EXPERIMENTAL ASSESSMENT OF PEDESTRIAN COMFORT IN URBAN ENVIRONMENT

EXTENDED ABSTRACT

A. Silveira Castanho[1]

1: Instituto Superior Técnico, DECivil, UTL, Av. Rovisco Pais, Lisboa, Portugal
E-mail: andrefs.castanho@gmail.com

October 2012

EXPERIMENTAL ASSESSMENT OF PEDESTRIAN COMFORT IN URBAN ENVIRONMENT

EXTENDED ABSTRACT

A. Silveira Castanho[1]

1: Instituto Superior Técnico, DECivil, UTL, Av. Rovisco Pais, Lisboa, Portugal
E-mail: andrefs.castanho@gmail.com

1. INTRODUCTION

Time after time, the buildings surrounding areas have been questioned due to the adverse comfort and safety conditions that can occur at pedestrian-level [1]. The wind action manifests itself at the pedestrian-level basically in two ways: either it can be felt as a wind speed which affects the rate of heat exchange between people and the environment; or as a force that comes from the sum of pressure field incident on human body [2]. The wind flow has multiple effects, including heat transfer by convection, penetration of rain, the dilution of the pollutants, noise or dust removal. The most significant effects on pedestrian are the mechanical and thermodynamic effects. This article only addresses the mechanical effects, noting that according to Lopes et al [3], the threshold of thermal comfort corresponds to wind speeds around 4,5 m/s. The pedestrian comfort depends on several parameters among which stand out, in addition to wind speed (and bursts critical speed), the local climate and the season, the environment temperature, rainfall, humidity, people activity on public environment, clothing and factors, such as, age and psychological state of each other. A preliminary evaluation of the wind behaviour at the ground level and around buildings can avoid the appearance of excessive wind-speeds. In this context, both buildings demolition and construction may change the optimum conditions of the wind flow [4]. When evaluating the discomfort associated with pedestrian-level wind, it is necessary to study the phenomena occurring at heights below 2 meters and the speed average obtained in the period between 10 minutes and 1 hour. In fact, according to Bottema [5], pedestrian discomfort happens whenever the wind effects become so strong and frequent (periods less than 1 hour) that people who are feeling these effects act to avoid them. A variety of solid bibliography is available on this subject, since the 60's of last century, of which it can be highlighted the studies conducted by Stathopoulos *et al*. [6]. Experimental studies were conducted considering the pedestrian-level wind flow in the vicinity of idealized buildings detailing the adjacent buildings areas. In these studies, the effect of the buildings characteristics, such as clusters of buildings and urban canyons (street canyons), was analysed, which allowing a preliminary assessment about wind speeds around buildings. However, few investigations have focused on areas around a group of buildings. Other studies have concluded that there is a relationship between wind speed and pedestrian-level comfort. The present work aims to assess the inter-relationship between the adverse conditions that buildings induce at pedestrian-level. As the wind at this level may affect pedestrian comfort, this study can leads building designers to provide better comfort control. An urban environment

boundary layer was simulated in a wind tunnel and then the wind flow effects on ground level was evaluated – by a scour method and a hot wire anemometer – for different buildings arrangement in a regular 3x3 mesh. The general characteristics of the flow at pedestrian-level height were investigated and experimentally tested for different arrangements of buildings heights and gap widths, in order to identify the locations and buildings arrangements which lead to more uncomfortable situations.

The effect of wind around buildings depends not only on topography and roughness of the surface, but also on the building's geometry, the layout of surrounding buildings and the wind direction. Consequently, there are some turbulence zones, sharp flow deflections on geometry changes (such as corners, edges, protrusions and recesses) and strong accelerations due to the flow confinement, whose effects are locally bounded and difficult to account for. Special attention should be given to these localized effects, especially when dealing with areas where comfort, that may reach pedestrian safety, may be compromised. These situations of potential pedestrian discomfort should be identified and corrected in the design phase. The goal of this paper is to evaluate (through wind tunnel testing) the influence of buildings layout in the urban pedestrian-level comfort. An experimental campaign was conducted on a small-scale model comprising a set of nine rectangular buildings arranged in a regular grid of three rows and three columns. An urban boundary layer was simulated for runoff incidence and preceded to the identification of potential zones of discomfort through a scour method to evaluate the flow velocity field at ground level. Additionally hot wire anemometers were used to determine mean wind speeds at predefined zones. A set of different buildings heights arrangements were tested and locations with critical zones around the buildings were identified obtaining a better understanding of geometry impact and buildings arrangements on pedestrian comfort.

2. TESTS METHODOLOGY

2.1 Atmospheric Boundary Layer

The mean wind speed increases with distance from the ground to a certain level, from which stabilizes, forming a atmospheric boundary layer (ABL) flow. The cause for such behaviour is the friction caused by the surface cover thereby causing a viscous stress of greater or lesser extent in the free air flow and so conditioning the mean wind speed and direction at the ground level. Thus, at a sufficiently large height, wind is not disturbed and assumes uniform speed. This uniform speed is the so-called velocity gradient at the boundary layer height (δ) that varies between 300 to 600 meters, depending on the roughness. Figure 1 illustrates the evolution of a boundary layer for three roughness characteristics (urban, suburban and sea).

In the study of wind actions, it is appropriate to decompose the instantaneous velocity $U(t)$ in the longitudinal sum of the mean wind speed $\bar{U}$ with the fluctuation around the mean speed $u(t)$, caused by turbulence phenomena in the interval time. It is noted that the effect of a wind gust affects pedestrian-level is more aggressive the buoyant portion is larger than the average for bursts having the same order of magnitude full speed [8].

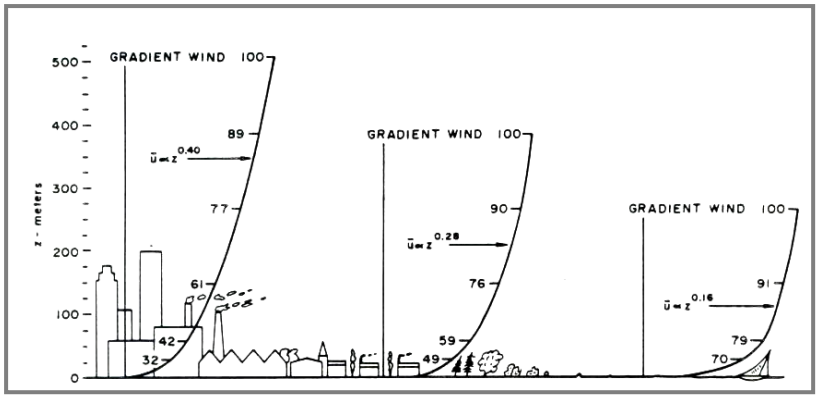

Figure 1 - Atmospheric boundary layer with different roughness [7].

Take as valid the following expression for the portion of the longitudinal velocity:

$$U(t) = \bar{U} + u(t) \tag{1}$$

For the description of the atmospheric boundary layer profile, there is a relationship between the logarithmic type, eq. (2):

$$\bar{U}(z) = \frac{u^*}{\kappa} \ln\left(\frac{z}{z_0}\right) \tag{2}$$

where z is the height above ground level, z_0 the surface scale roughness, κ the *Von Karman* constant, which assumes the approximate value of 0,4, and u^* the friction velocity, which can be expressed by:

$$u^* = \sqrt{\frac{\tau_0}{\rho}} \tag{3}$$

τ_0 being the shear stress between air and the surface and ρ, the fluid density.

The mean wind-speed profile along the surface boundary layer may also be described by a power law that was firstly used to describe the variation of mean wind speeds in homogeneous surface land,

$$\bar{U}(z) = \bar{U}_{ref}\left(\frac{z}{z_{ref}}\right)^{\alpha} \tag{4}$$

where $\bar{U}_{ref}$ is the mean wind-speed measured at the reference point z_{ref} and α the exponent α that depends on the type of terrain (aerodynamic roughness).

Speed fluctuations in compared to its average value are closely related to the turbulence of the wind flow, as they are dependent on the creation, movement and vortices abolition, based on the *Taylor* hypothesis. These vortices move with the mean flow velocity and with flow's direction of propagation. The atmospheric turbulence is characterized by its intensity, defined as:

$$I_i(z) = \frac{\sigma_i(z)}{\bar{U}_z} \quad (i = u, v, w) \tag{5}$$

where $\sigma_i(z)$ refers to the standard deviation of three spatial fluctuating components of the wind *u* (longitudinal), *v* (lateral) and *w* (vertical) at a given average speed $\bar{U}_z$, at a distance *z* from the surface reference (ground-level) [9].

The wind speed and direction are two variables that do not assume a constant pattern over time due to the concept of turbulence that affects the air flow. At each moment, it can be defined a velocity field *U (u, v, w).* This paper only considers the dominant longitudinal wind speed, the longitudinal. Among other methods for simulation of a boundary layer (ABL) created at a wind tunnel, it was adopted the Irwin method [10]. A suburban type boundary layer was assumed for the study site, with a corresponding value of α = 0,23. Given the dimensions of the wind tunnel test – 9,0 × 3,1 × 2,0 m^3 , length × width × height – it was decided that the boundary layer would assume a uniform width span behaviour at a distance *x.h* , establishing the value of 4,5 for the x lower limit. The boundary layer height assumes a value of δ=1,0 m. Thus, the height of boundary layer is formed at about 50% of the wind tunnel height. In accordance to longitudinal direction, the boundary layer is fully developed at 5,5 m after the beginning of the test chamber. Among the possible combinations is chosen for the roughness elements, a cube of edge 10 cm, yielding an array of seven transverse rows of eight blocks, interspersed with six rows of seven blocks, with a wheelbase 40,0 cm corresponding to spacing between adjacent cubes of 30,0 cm. There are arranged in a staggered fashion, adopting spacing between two consecutive lines with a value equal to the spacing between cubes (Figures 2 and 3).

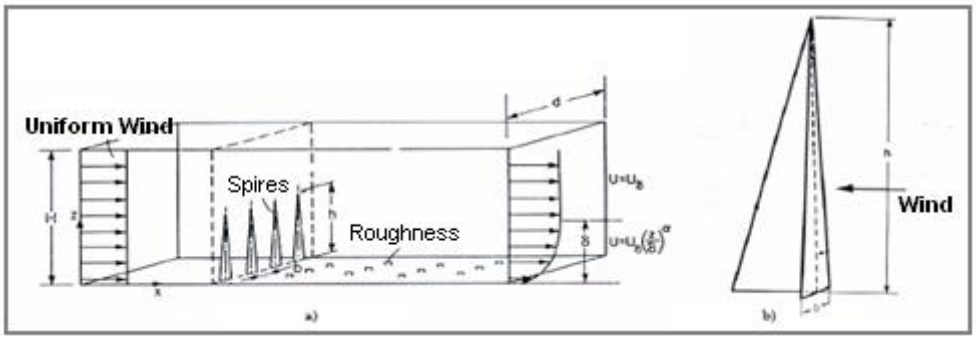

Figure 2 - a) Elements arrangement of that lead to the formation of atmospheric boundary layer height δ, b) triangular configuration of passive elements (spires) [3].

The Laboratório Nacional de Engenharia Civil (LNEC) wind tunnel, where the tests were conducted, is an open suction tunnel, i.e. without air recirculation, having a rectangular section with the dimensions cited above. It's a tunnel with six low-speed axial fans, 11 kW each, allowing wind speeds in the order of 3,5 m/s per fan. The following equipments (that allow quantitative measurement of flow) were used in the simulation: i) the *Pitot-Prandlt* tube, for determining the dynamic pressure, P_d, of the flow, from which is obtained the speed, eqs. (6) and (7); ii) micromanometer *van Essen*, *Betz* type associated with the *Pitot-Prandlt* tube for determining the reference dynamic pressure flow; iii) pressure transducer *PSI* ® , scanner *ESP HD* , combined with a data acquisition system *DTC Initium* ®.; and iv) hot wire anemometer ® *DANTEC* controlled by a *mini* ® *CTA* chain for the local measurements and evaluating the

turbulence intensity profile. The entire acquisition system is controlled by computer using dedicated software also allowing data storage for further processing.

Figure 3 - Roughness elements used on atmospheric boundary layer simulation.

In the first stage, the ABL characteristics were evaluated using two *Pitot* tubes : one on the test area, approximately 0,2 m from ceiling, which will measure, at all times, the reference speed, and one *Pitot* tube placed downstream of roughness, with variable height, in order to evaluate the wind speed profile. The dynamic pressure of flow, P_d (Pa) is defined by eq. (6) where ρ is the density of the fluid, in this case the air (ρ_{ar} = 1,23 kg/m^3), and v the flow speed (m/s),

$$P_d = \frac{1}{2}\rho v^2 \tag{6}$$

The v speed can then be obtained by,

$$v = \left[\frac{(P_0 - P_e)}{\rho} \times 2\right]^{\frac{1}{2}} \tag{7}$$

where P_0 is the total pressure and P_e is the environment static pressure. The averaged reference dynamic pressure was P_d = 30,88 Pa, corresponding to a $U \approx 7$ m/s speed. Figure 4 represents the velocity (α = 0,23) and turbulence intensity (β = - 0,18) profiles obtained in the first stage of the tests. The boundary layer has, upstream of the model, a thickness of δ=1,06 m.

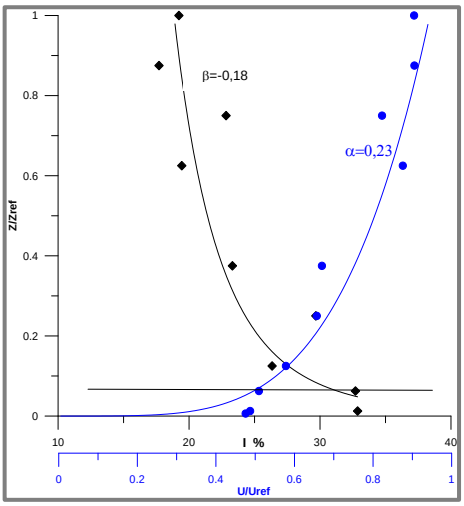

Figure 4 - Velocity profile (blue line and circles) and turbulence intensity (diamonds and black line), the horizontal line marks the ground-pedestrian level on analysis (2 meters).

2.2 Wind flow around buildings

The wind action of immersed obstacles in the atmospheric boundary layer is also a function of the characteristics of the obstacle: geometry, sharp edges, its size relative to other obstacles, or the spacing between them [9].

An important parameter to flow characterization is the *Reynolds* number (*Re*) that represents the ratio of the inertial forces to the viscous forces, defined as:

$$\mathrm{Re} = \frac{\rho \bar{U}^2 D^2}{\mu \bar{U} D} = \frac{\rho \bar{U} D}{\mu} = \frac{\bar{U} D}{\nu} \tag{8}$$

where *D* is a characteristic dimension of the obstacle, $\bar{U}$ the mean flow velocity and ν the air kinematic viscosity coefficient.

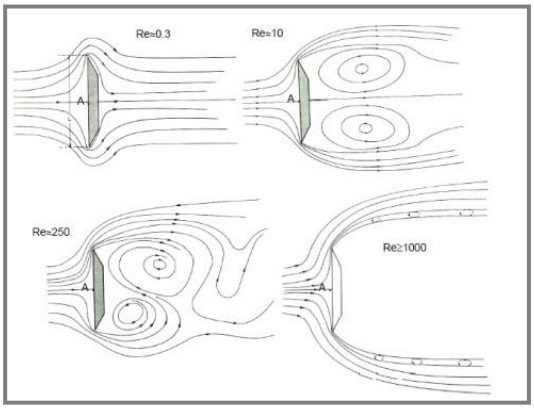

Figure 5 – Streamlines with different *Reynolds* number [11].

Figure 5 represents the flow streamlines around a plate edges. For *Re* ≈ 0,3 the viscous forces overcome the flow inertia forces, remaining adherent to the surface circumventing the windward and leeward faces. The flow separation (when the flow lines loose contact with the obstacle) starts with increasing speed, *Re* ≈ 10, when symmetrical vortices starts in plate leeside. For *Re* > 100, the inertial forces prevail over the viscosity, thus causing, in the plate leeside a region with fully separated turbulent flow and well-defined vortices. Separation points are dependent on the geometry of the body, being very marked in the presence of surface discontinuities as in the case of edges. In general, it can be concluded that, whenever a deceleration of the flow, caused by a positive pressure gradient ($dp / dx > 0$) and this is considerable for reversing the flow direction along the body walls (layer limit), separation occurs. The positive pressure gradient (adverse) may be observed in various situations by changing the direction of current lines (progressive – curved surfaces, or sudden – in sharp edges) or by the effect of the body viscosity causing a decrease in flow velocity close to the surface. This behaviour turns the flow independent of Re, making tests easier to keep similarity conditions. Figure 6 shows, for a relatively simple case, the flow around an isolated building subjected to a boundary layer flow, normal to one facade. Positive pressures are shown in the building front facade, while suctions, i.e. negative pressures, are observed in lateral, rear and top regions, as a result of the phenomenon of flow separation on the edges. The vortexes at the bottom of the building facade

are conveyed with high speed in the direction of the vertical edges of the building, bypassing them. At pedestrian level, these areas are often uncomfortable.

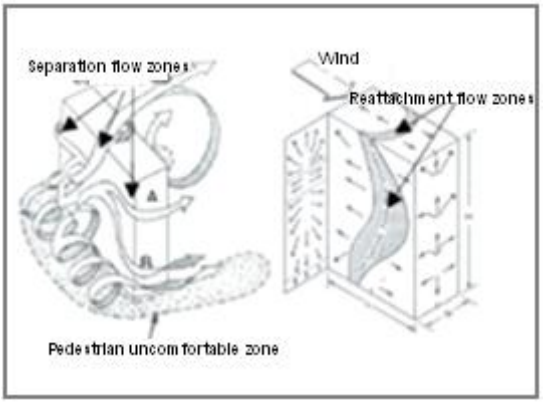

Figure 6 - Flow characteristics around an obstacle subjected to a boundary layer flow [12].

Note that when the longitudinal dimension of the obstacle is sufficiently large (*L*> *4H*) flow regains contact with the surface (reattachment). Front surface stagnation occurs at ≈ 70% of the height (with atmospheric boundary layer flow), resulting in a downwash flow on the lower 2/3, and an upward flow in the upper third, Figure 6.

2.3 Case study

The physical model consists on a 3 × 3 matrix arrangement of buildings, made out of a set 7,5cm length (*L*) cubes. The obstacles are characterized by a width (*B*) and height (*H*) in three rows (*i* = 1, 2, 3) perpendicular to the direction of the incident flow and three columns (*j* = 1, 2, 3) in the longitudinal direction. In this way, four case studies were considered:

- Case 1: $B_{i,j} = H_{i,j} = Gap = L$;
- Case 2: $B_{i,j} = Gap = L \quad e \quad H_{i,j} = 2L$;
- Case 3: $B_{i,j} = Gap = L \quad e \quad H_{1,j} = H_{2,j} = \frac{L}{2}$, $H_{3,j} = 2L$;
- Case 4: $B_{i,j} = Gap = L \quad e \quad H_{1,j} = H_{2,j} = L$, $H_{3,j} = 2L$;

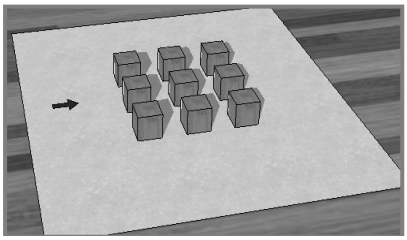

Figure 7 – Case 1 (3xLxLxL)

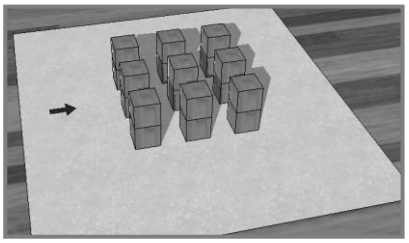

Figure 8 – Case 2 (3xLxLx2L)

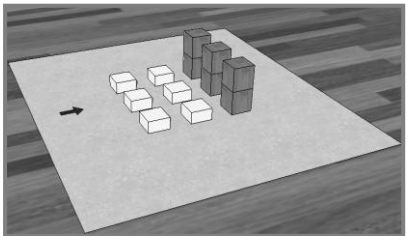

Figure 9 – Case 3 ((2xLx0.5L)+(1xLx2L))

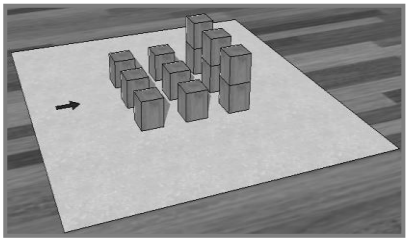

Figure 10 – Case 4 ((2xLxL) + (1xLx2L))

2.4 Wind speed analysis

A technique developed at the Laboratório Nacional de Engenharia Civil (LNEC) based on evaluation of friction stress fields caused by runoff and contact of solid particles with the ground [13] was used in this work. This scour method allows evaluating the consequences of wind flow acting on ground level surfaces and velocity field characteristic [13]. This method consists in spreading a uniform layer of solid and loose particles on the surface to be assessed. The most commonly used solution uses sand particles of defined granulometry (sand is passed through series of ASTM sieves, and its dimension are defined by the mesh of the sieve on which it is retained) over a thin cork layer covering the area under study. The small size particles (not overlapped) performs a layer, subjected to a so-called viscous sub-layer of the wind boundary layer flow, which are moved by drag mechanisms (not jumping movements) occurring when the value of the force resulting from drag (function of flow velocity) exceeds the frictional force of the sand particles with the cork surface. Otherwise, the particles remain in the same position in which they are initially placed or those being in motion cease their movement when the frictional force overcomes the drag force. The sand particles thereby forms well defined figures (of eroded sand) whose contour corresponds to the precise balance between these two forces, based on the following condition:

$$C_d \frac{1}{2} \rho . U_{ref}^2 A_{ref1} = \tau_0 A_{ref2} \tag{9}$$

where C_d is the drag coefficient of the particles for a given mean speed flow U_{ref} at a given level above the ground, ρ is the density of air, A_{ref1} is a reference area, normally corresponding the area to the projection of the particle in a surrounding vertical plane, A_{ref2} is a reference area and τ_0 is the shear stress at the wall. Note that the shear stress depends on the nature and type of materials involved. Moreover, as the friction velocity (the speed characteristic of the surface), u^*, is defined by eq. (3), it is understandable that the boundary area (border) of each erosion figure is a zone of constant velocity and, as the friction velocity at each point of the surface is directly related to the incident flow velocity:

$$\frac{u_1^*}{u_2^*} = \frac{U_1(z)}{U_2(z)} = \gamma \tag{10}$$

i.e., the relationship between friction speeds γ of two erosion figures, for any pair of points on the surface, is identical to the ratio of the incident flow velocities (to a predetermined reference level) that gave them origin [13].

The technique requires a preliminary test in order to evaluate a reference wind speed, being taken as the reference condition corresponding to the starting point of sand movement with no obstacles present. The wind tunnel test area is coated with a 1 mm thick cork layer with dimensions of 1,0 × 0,80 m^2, where sand grains (size 50) was uniformly spread. The mesh cubes for testing, with edge L = 7,5 cm, considered an arrangement with spacing (gap) between cubes in x and y, equal to L. The reference wind speed is achieved in this experimental

procedure from dynamic pressures measured within the tunnel (by a *Pitot* tube) in the order of 43 Pa, corresponding to speed values of about 8,4 m/s. The last stage of the experiment consisted in measuring flow speeds, using the hot wire anemometer in pre-set and strategic points, to evaluating the pedestrian comfort at 2 meters height (5 mm on this model), as well as evaluation of local turbulence levels.

3 RESULTS

3.1 Scour method

For each of the cases tested, the erosion figures are obtained as a function of γ parameter (eq. 10), corresponding to the ratio of the undisturbed speed flow of each test, and the reference wind speed. It should be clear the meaning of γ, matching its value to the mean wind speed for each display value. Hence, γ = 0,86 means that in order to have the speed limit comfort at ground level, for example 4,5 m/s, the incident wind speed will be 3,87 m/s turning the zone more vulnerable, increasing the probability of exceedance. If γ = 1,07 it means that the incident wind speed is 4,8 m/s, conferring to this point a (slightly) protected zone. Therefore, areas where removed sand particles correspond to values of γ < 1 are more exposed to wind, and more prone to situations of discomfort.

3.1.1 Case 1

The corner effects (edge separation) begin to show at the level of the first line to a speed flow corresponding to γ = 0,87 (Figure 11), keeping the remaining shielded (sheltering effect). Accelerating the flow (γ to achieve the unit value) erosion figures begin to draw up at level of the second and third rows, being their dimensions inverse to the distance to the first row of the model. Thus, the third row is more protected by upstream buildings.

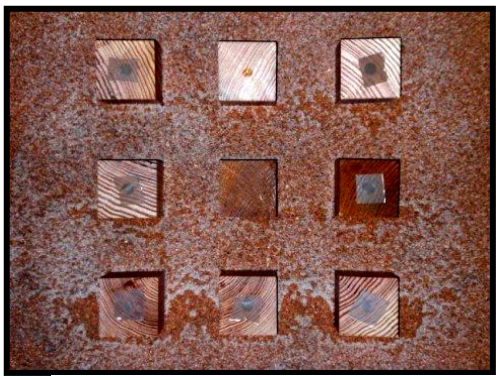

Figure 11 - Case 1 (γ = 0,87).

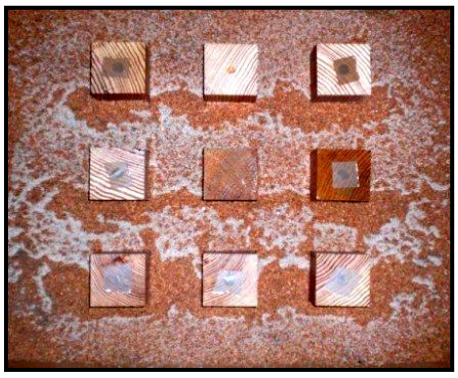

Figure 12 - Case 1 (γ =1,07).

For wind speed values close to the reference, the separation starting from the upstream edge propagates to the last rows. When the reference speed is exceeded (Figure 12) the erosion pictures are most evident, concluding that the effect of gap (channel effect) is most pronounced at the first row of buildings. It is emphasized symmetry in figures on the central block of buildings.

3.1.2 Case 2

In this case, the formation of erosion figures occurs at lower speeds, γ = 0,70 (Figure 13). The corner effect is more pronounced, but remains only in the first row of buildings. For γ = 0,86 erosion completely surrounds the first row and extends to the other two (Figure 14) what can be explained by the influence of the height of the buildings, keeping the width and length of the streets between the buildings. The sweep of the sand particles turns to be very strong when wind speed reference is reached, a fact which progressively leads to some uncertainty in the contours.

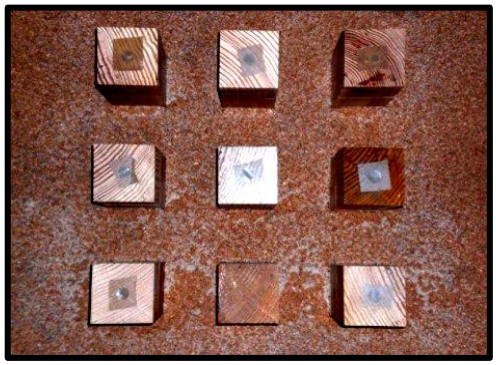

Figure 13 - Case 2 ($\gamma = 0,70$).

Figure 14 - Case 2 ($\gamma = 0,86$).

3.1.3 Case 3

For γ = 0,70, there is a corner effect at all buildings but it is clearly larger around taller buildings on the third row (Figure 15), as well as the street canyon effect. The increasing of the flow speed (Figura 16) induces a larger corner effect of first row, in a process similar to case 1. Also to be noted is the extension of the discomfort zones of around the tallest buildings row in analogy to centre line buildings. In this way, last row buildings experiment almost complete swept of the sand particles on ground level environment.

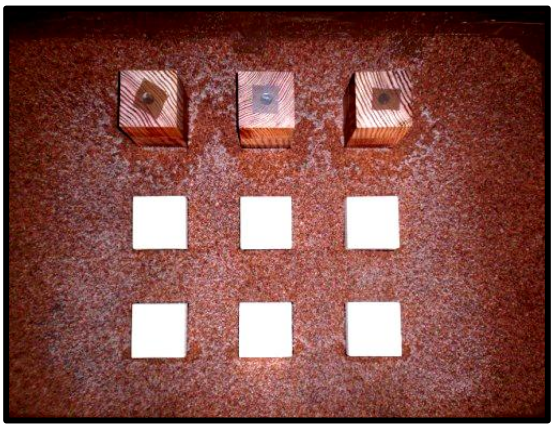

Figure 15 - Case 3 ($\gamma = 0,70$).

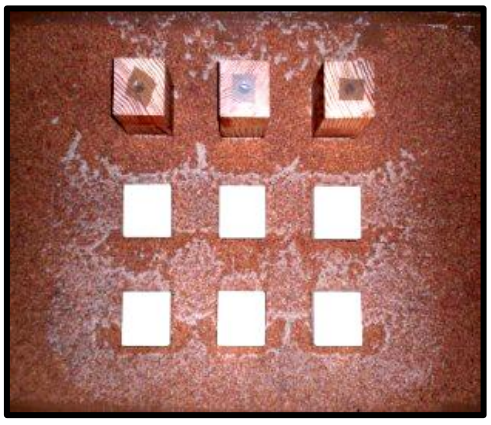

Figure 16 - Case 3 ($\gamma = 1,00$).

3.1.4 Case 4

For wind speeds lower than the reference, corner effects are observed, both in the front and last rows, the tallest buildings being the most affected (Figure 17). The pattern found in case 2, is repeated here for the first two rows, allowing to conclude that a change on buildings height in the last row does not propagate upstream. However, it appears that the buildings height influences the forward shield effect on the tallest buildings. In this point of view, for equal wind speeds, the effects are less noticeable compared to the case 3. Along the central row of buildings (γ = 0,88) erosions were not significant (Figure 18). It is for reference speed, γ = 1,00 that perfectly symmetrical erosion figures rise, eroding the surrounding area of all buildings combining a corner effect with a downwash in their frontal facades. Figure 19 shows the contours of erosion figures when the flow is accelerated about 7% (γ=1,07).

Figure 17 - Case 4 ($\gamma = 0{,}70$)

Figure 18 - Case 4 ($\gamma = 0{,}88$)

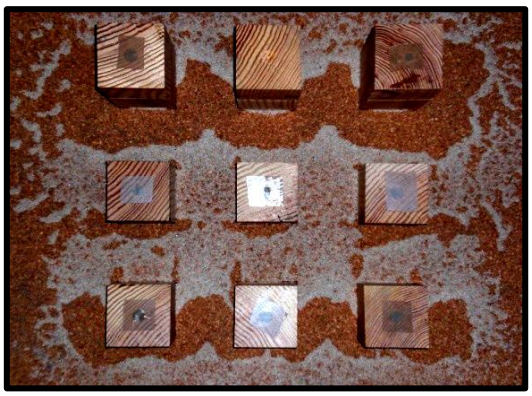

Figure 19 - Case 4 ($\gamma = 1{,}07$)

3.2 Hot wire anemometer

Figure 20 shows the longitudinal axes where the wind speed results relatively to the undisturbed flow (x/X_{tot} = 0) were obtained, with the hot wire anemometer at an elevation of 2,0 meters (where the black block represents the relative positions of buildings).

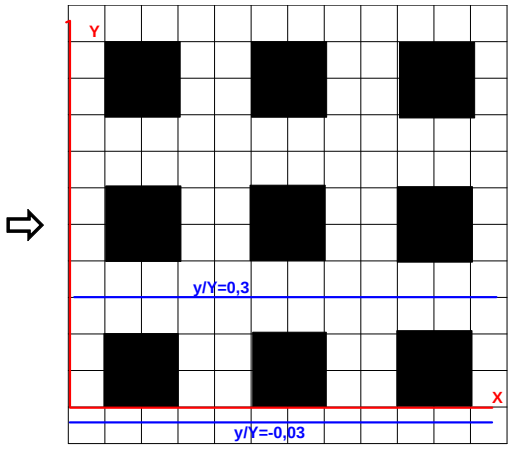

Figure 20 – Axes for hot wire measurements.

The channel effect is evident (Figure 21) in the first row for all cases (x/X_{tot} ≈ 0,4), and also downstream from the last row of buildings in Case 3. Figure 22 shows some notable points such as accelerations registered in Case 1 (for x/X_{tot} ≈ 0,4), but in agreement with that shown in Figure 12, and in Case 4 (for x/X_{tot} ≈ 1,0) also in agreement with Figure 18 .

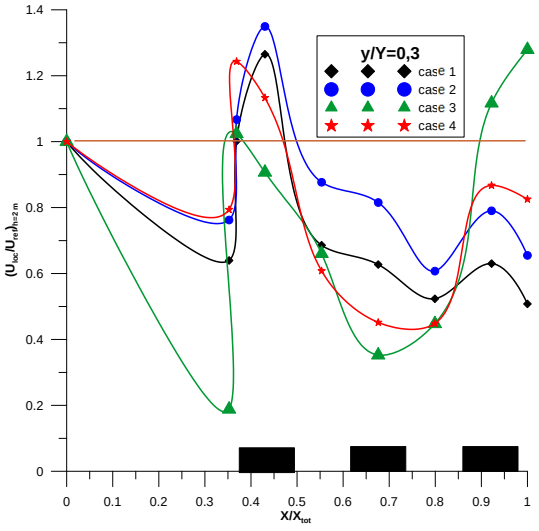

Figure 21 – Hot wire results to y/Y=0,3.

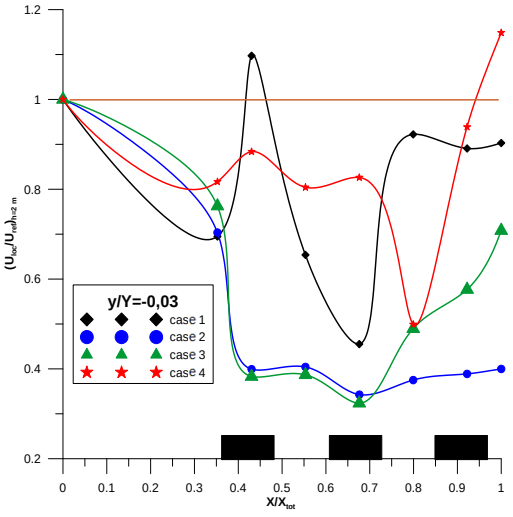

Figure 22 – Hot wire results to y/Y= - 0,03.

Some experimental results of local speeds at 2 meters elevation, obtained with hot wire anemometers, were also compared with numerical results in CFD (Computational Fluid Dynamics) carried out by Moret Rodrigues *et al.* [14]. It was observed that the agreement between the experimental and numerical results was satisfactory, both in terms of speed values as the trend curves. This agreement is higher for cases 1 (y/Y_{tot} = 0,3) and 2 (y/Y_{tot} = - 0,03) – Figures 23 and 24 - and lowest for cases 4 and 5 for y/Y_{tot} = - 0,03 – Figures 25 and 26 -, because it might be also considered other directions of the velocity field (*v* and *w*).

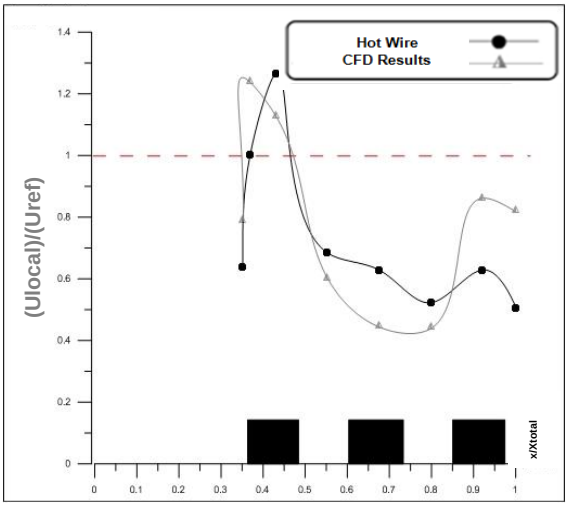

Figure 23 – Comparison between hot wire results and CFD to Case 1 - y/Y_{tot}=0,3.

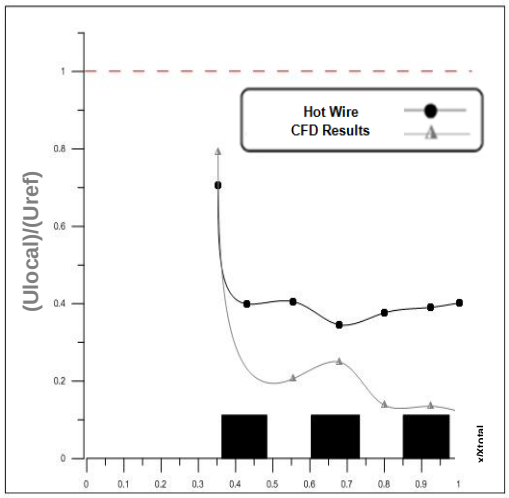

Figure 24 – Comparison between hot wire results and CFD to Case 2 - y/Y_{tot}=-0,03.

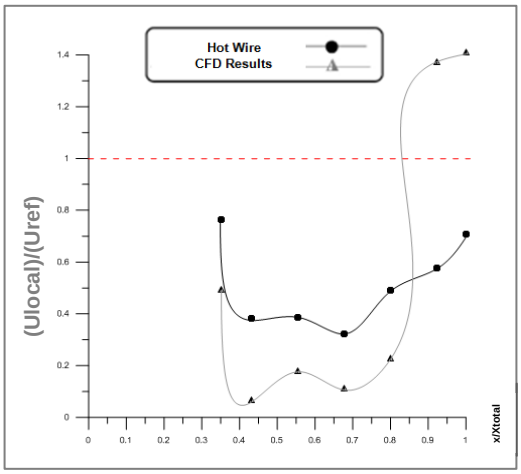

Figure 25 – Comparison between hot wire results and CFD to Case 4 - y/Y_{tot}=- 0,03.

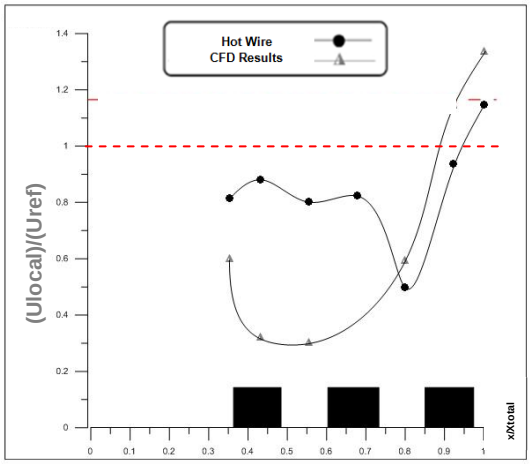

Figure 26 – Comparison between hot wire results and CFD to Case 5 - y/Y_{tot}=- 0,03.

4. CONCLUSIONS

The identification of potential pedestrian discomfort situations is of outmost importance for the definition of urban design. The configuration of some buildings and their relative positions allow the development of intense flows that cause discomfort at ground level. It will always be a task for designers to choose the optimal configuration so there is no runoff and unpleasant wind speeds for pedestrians. The knowledge gained provides useful guidance for the architect/engineer in the design phase. In this way, there are two main types of flow which adversely affect the pedestrian environment, i.e. descending flows and horizontally accelerated flows. In this paper, the phenomena that increase the wind velocity near the buildings were analysed, such as the corner effect, the channel (street canyon) effect and the downwash effect. It was found that the pedestrian-level discomfort increases with the building height, due to the increasing of the downwash effect. Unlike the buildings which contain arrays of very similar dimensions, in which the pedestrian areas are generally protected, in cases 3 and 4, there are problems of pedestrian discomfort. The cause of this behaviour is that the flow from

the lower (upstream) buildings collides with the front of tall buildings, originating a downwash effect that reaches the ground-level in front of the third row of buildings. In case 3, the accelerations are most significant at the last row of buildings, being accompanied by a strong channel effect. In case 4, as the ratio between the heights of the buildings of the first two rows and the last is smaller, the effect is less pronounced. The configuration of case 2 intended to evaluate the influence of the ratio increase between the height and width of the building gaps. The effect of channel is much more pronounced in case 2 than in case 1 with half-height buildings, causing movement harshest conditions.

REFERENCES

[1] Wu, Hanqing. Pedestrian – Level wind environment around buildings. Montreal, Québec, Canadá, Concordia University, 1994.

[2] BÊNIA, Maria Cristina Dolz. Criteria Evaluation for determining people's comfort and safety conditions facing wind action. 2010. 139 f. Dissertação (Grau de Mestre) - Departamento de Escola de Engenharia, Universidade Federal do Rio Grande do Sul, Porto Alegre, 2010 (in portuguese).

[3] Lopes, A.; Oliveira, S.; Marques da Silva, F.; Saraiva, J., "Thresholds of comfort from tests in the wind tunnel: First results." "Lisbon: Cities and Climate Changes. What Future?", Universidade de Lisboa, 15-16 Maio, 2008 (in portuguese).

[4] Design guide for wind, District Plan - Volume 2: Design Guides, Non-statutory: For Guidance Only, 2000.

[5] Bottema, M. (2000). A method for optimisation of wind discomfort criteria, *Building and Environment*, 35: 1-18.

[6] Stathopoulos, T., Wu, H. and Bedard, C., "Wind Environment Around Buildings: A Knowledge-Based Approach", Journal of Wind Engineering and Industrial Aerodynamics, 41–44: 2377–2388, 1992.

[7] H. P. Irwin – The Design of Spires for Wind Simulation – Journal of Wind Engineering and Industrial Aerodynamics, 7, pp. 361-366, 1981.

[8] Yu, Johnny T. S., Che, Ping, Road Wind effects on pedestrians, Fanling, Hong Kong. in Proceedings of the Fourth International Conference on Wind Effects on Buildings and Structures, London, 1975, Cambridge Univ. Press, Cambridge, 1976, pp. 403-422.

[9] M.G. Gomes, Wind effects on buildings. Experimental evaluation of pressure coefficients for L- and U- shaped buildings, McS Thesis, Instituto Superior Técnico (IST), Technical University of Lisbon (2003) (in portuguese).

[10] Potter, M.; Wiggert, D. – "Mechanics of fluids", Prentice-Hall International, Inc, 1991.

[11] Simiu, E.; Scanlan, R. – "Wind effects on structures. An introduction to wind engineering", John Wiley & Sons, 3rd Edition, 1996.

[12] ASHRAE, "Handbook – Fundamentals", ASHRAE, Atlanta, 1993.

[13] Janeiro Borges, A. R.; Saraiva, J. G. (1980), "An erosion technique for assessing ground level winds", Wind Engineering, 1 - 5th Int.Conference on Wind Eng. Research, Fort Collins, CO, Pergamon Press, 235-242 (in portuguese).

[14] Moret Rodrigues, A.; Gomes, M. Glória; Canha da Piedade, A. (2003), "Wind environment around building complexes", Proceedings of the 5th International Conference on Urban Climate (ICUC5), Lodz, Poland, 1-5 September 2003, pp. 447-450 (in portuguese).